Measurement report: Diurnal variations of brown carbon during two distinct seasons in a megacity in Northeast China

Yuan Cheng[1], Xu-bing Cao[1], Jiu-meng Liu[1,*], Ying-jie Zhong[1], Qin-qin Yu[1], Qiang Zhang[2] and Ke-bin He[3]

[1] State Key Laboratory of Urban Water Resource and Environment, School of Environment, Harbin Institute of Technology, Harbin 150090, China

[2] Ministry of Education Key Laboratory for Earth System Modeling, Department of Earth System Science, Tsinghua University, Beijing 100084, China

[3] State Key Joint Laboratory of Environment Simulation and Pollution Control, School of Environment, Tsinghua University, Beijing 100084, China

[*]Corresponding author. Jiu-meng Liu (jiumengliu@hit.edu.cn).

Abstract

Brown carbon (BrC) represents an important target for the "win-win" strategy of mitigating climate change and improving air quality. However, estimating co-benefits of BrC control remains difficult for China, partially because current measurement results are insufficient to represent the highly variable emission sources and meteorological conditions across different regions. In this study, we investigated, for the first time, the diurnal variations of BrC during two distinct seasons in a megacity in Northeast China. The winter campaign conducted in January of 2021 was characterized by low temperatures rarely seen in other Chinese megacities (down to about –20 °C). The mass absorption efficiencies of BrC at 365 nm (MAE_{365}) were found to be ~10% higher at night. The variations of MAE_{365} could not be explained by the influence of residential biomass burning emissions or secondary aerosol formation, but were strongly associated with the changes of a diagnostic ratio for the relative importance of coal combustion and vehicle emissions ($R_{S/N}$). Given that most coal combustion activities were uninterruptible, the higher nighttime MAE_{365} in winter were attributed primarily to increased emissions from heavy-duty diesel trucks. The spring

26 campaign conducted in April of 2021 was characterized by frequent occurrences of agricultural fires,

27 as supported by the intensive fire hotspots detected around Harbin and the more-than-doubled

28 levoglucosan to organic carbon ratios (LG/OC) compared to winter campaign. In spring, MAE_{365}

29 depended little on $R_{S/N}$ but exhibited a strong positive correlation with LG/OC, suggesting open

30 burning emissions as the dominant influencing factor for BrC's light absorption capacity. MAE_{365}

31 were ~70% higher at night for the spring campaign, pointing to the prevalence of nighttime

32 agricultural fires, which were presumably in response to local bans on open burning. It is noteworthy

33 that the agricultural fire emissions resulted in distinct peak at ~365 nm for the light absorption

34 spectra of BrC, and ~~a~~ candidates for the compounds at play ~~was~~ were inferred to be aromatic species

35 with nitro-functional groups ~~$C_7H_7NO_4$~~. ~~Due to the presence of the ~365 nm peak, the absorption~~

36 ~~Ångström exponents could not be properly determined for the agricultural fire-impacted samples.~~

37 The presence of the ~365 nm peak complicated the determination of absorption Ångström exponents

38 for the agricultural fire-impacted samples. In addition, the ~365 nm peak became much less

39 significant during the day, likely due to photo-bleaching of the relevant chromophores.

1. Introduction

Light-absorbing organic carbon, i.e., brown carbon (BrC), exerts important yet poorly understood effects on climate and the environment (Brown et al., 2018; Zeng et al., 2020; Sand et al., 2021). As a mixture of numerous organic compounds from both primary emissions and secondary formation, BrC exhibits extreme complexity in spectroscopy, composition and evolution (Laskin et al., 2015; Brege et al., 2021; Washenfelder et al., 2022). Measurement techniques for BrC absorption mainly fell into two categories, including solvent extraction followed by light absorption spectrum measurement (Chen and Bond, 2010; Hecobian et al., 2010) and apportionment of total aerosol absorption to the contributions from black carbon and BrC (Yang et al., 2009; Lack et al., 2012). So far, consistency between BrC results from these two types of approaches has not been addressed, with variable relationships, either linear or non-linear, and unclear influencing factors (Kumar et al., 2018; Zeng et al., 2022). This inconsistency introduced substantial difficulties to the integration of BrC measurement results across studies and regions (Wang et al., 2022), which is essential for unfolding the links between BrC sources and optical properties. In addition, efforts were also made to explain BrC absorption on a molecular level. Several techniques were shown to be powerful, such as electrospray ionization Fourier transform ion cyclotron resonance mass spectrometry (ESI FT-ICR MS; Wozniak et al., 2008; Jiang et al., 2021; Zeng et al., 2021), high performance liquid chromatography coupled with high resolution mass spectrometry (HPLC/HRMS; Lin et al., 2018; Huang et al., 2022; Xu et al., 2022), and two-dimensional gas chromatography with time of flight mass spectrometer (GC×GC-ToF-MS; Huo et al., 2021). These techniques were more frequently applied to laboratory-generated primary or secondary BrC (e.g., Lin et al., 2015), which usually had less complex composition than ambient BrC and thus showed

62 relatively high fraction of resolvable chromophores, e.g., up to ~85% for those emitted by biomass

63 burning (Huang et al., 2022).

64   The absorbing nature of BrC makes it a non-negligible contributor to positive radiative forcing

65 (Saleh, 2020), while the considerable contribution of organic aerosol to fine particulate matter

66 ($PM_{2.5}$) makes BrC an important source of air pollution (Wang et al., 2019). Consequently, BrC

67 represents a key species for the "win-win" strategy of mitigating climate change and improving air

68 quality. Given the highly variable emission sources and meteorological conditions across different

69 regions in China, field observational results on BrC are far from being enough to constrain air

70 quality and climate models, limiting the ability to evaluate the co-benefits of BrC control. In this

71 study, we focused on a largely unexplored city cluster, the Harbin-Changchun (HC) metropolitan

72 area in Northeast China. Compared to other regions with intensive studies of BrC as well as other

73 air pollutants (e.g., the North China Plain), HC was characterized by extremely cold winter and

74 strong impacts of biomass burning on top of other anthropogenic emissions (e.g., from coal

75 combustion). The first feature was related to the relatively high latitudes of HC. For example, as the

76 northernmost megacity in China, Harbin has an average temperature of about –20°C in January,

77 significantly lower than that of Beijing (~0 ℃). The second feature was related to the massive

78 agricultural sector in HC. Until recently, open burning was still an irreplaceable approach for the

79 disposal of crop residues in this region, presumably because the amount of agricultural wastes was

80 too huge for the capacity of sustainable use. The agricultural fires frequently resulted in heavily-

81 polluted episodes with high $PM_{2.5}$ concentrations rarely encountered in other Chinese megacities

82 (e.g., hourly-average of ~1000 $\mu g/m^3$ in Harbin; Li et al., 2019). These two features highlighted the

83 uniqueness of HC for haze studies in China.

84   This measurement report, for the first time, presented field observational results on the diurnal

85   variations of BrC during two distinct seasons, i.e., a frigid winter and an agricultural fire-impacted

86   spring, in the central city of HC. Drivers for the diurnal variations were discussed based on

87   indicators of various sources. Particularly, the agricultural fires were found to result in unique

88   absorption spectra of brown carbon. This study provided implications for parameterization of BrC

89   in climate models.

90   **2. Methods**

91   **2.1 Field sampling**

92   Daytime and nighttime $PM_{2.5}$ samples were collected on the campus of Harbin Institute of

93   Technology (HIT) during winter and spring of 2021. HIT was surrounded by residential and

94   commercial areas, without major industrial sources nearby, and thus represented a typical urban site.

95   The sampling was done by a mass flow controlled high-volume sampler (TE-6070BLX-2.5-HVS;

96   Tisch Environmental, Inc., OH, USA), which was operated at a flow rate of 1.13 m^3/min using pre-

97   baked quartz-fiber filters ($8'' \times 10''$, 2500 QAT-UP; Pall Corporation, NY, USA). To avoid rush hours

98   and considering the relatively early sunset time in winter (~16:00–17:00), ~~Daytime~~ daytime and

99   nighttime samples were collected from 9:00 to 16:00 and from 21:00 to 5:00 of the next day,

100   respectively. The winter campaign covered the entire January of 2021, and the spring campaign was

101   conducted during 10–30 April, 2021.

102   **2.2 Laboratory analysis**

103   Two punches with diameters of 20 mm were taken from each sample, combined and then

104   extracted by deionized water. The water extract was analyzed using a Dionex ion chromatography

105   system (ICS-5000$^+$; Thermo Fisher Scientific Inc., MA, USA). Levoglucosan, an organic tracer for

106   biomass burning, was determined by the high-performance anion-exchange chromatography

107   coupled to pulsed amperometric detection (HPAEC-PAD) method (Engling et al., 2006; Yttri et al.,

108   2015). Inorganic ions such as nitrate, sulfate, chloride, ammonium and potassium were also

109   measured. Linear regression of the total cation concentration on that of total anion (both in µeq/m^3)

110   led to a slope of 1.14 ±0.01 (intercept was set as zero; $r = 0.99$), indicating a neutralized feature of

111   the Harbin aerosols.

112   Two punches with diameters of 47 mm were taken from each sample and used to determine

113   carbon fractions. Following the method developed by Chen and Bond (2010) and refined by Cheng

114   et al. (2016), one punch was directly measured for organic carbon and elemental carbon, while the

115   other punch was immersed in methanol (HPLC grade; Fisher Scientific Company L.L.C., NJ, USA)

116   for an hour without stirring or sonication, dried in air for another hour, and then analyzed. Both

117   punches were measured by a Thermal/Optical Carbon Analyzer (DRI-2001; Atmoslytic Inc., CA,

118   USA), which was operated with two commonly-used temperature protocols (i.e., IMPROVE-A and

119   NIOSH) and transmittance charring correction. The difference of total carbon (TC) concentrations

120   between the untreated and extracted punches ($TC_{untreated} - TC_{extracted}$) was used to represent the

121   amount of organic carbon that is soluble in methanol (MSOC)~~, following the method developed by~~

122   ~~Chen and Bond (2010) and refined by Cheng et al. (2016)~~. Given that the TC measurement was

123   independent of the temperature protocol used, both $TC_{untreated}$ and $TC_{extracted}$ were determined as the

124   averages of total carbon results from IMPROVE-A and NIOSH. A benefit of this approach was that

125   the uncertainty of MSOC (σ) could be estimated for each sample based on the parallel TC

126   measurements by different protocols:

127      $$\sigma = \sqrt{\left(\text{SD of } TC_{untreated}\right)^2 + \left(\text{SD of } TC_{extracted}\right)^2} \Big/ \left(TC_{untreated} - TC_{extracted}\right)$$

128   where SD indicates standard deviation. In this study, σ averaged 3.3 $\pm$2.9% with a median of 2.4%.

129   In addition, organic compounds that are in-soluble in methanol, i.e., MIOC, was measured as the

130   organic carbon concentration of the extracted punch. Unless stated otherwise, (i) OC involved in

131   the following discussions indicates the sum of MSOC and MIOC, and correspondingly, EC indicates

132   elemental carbon measured by the extracted punch; and (ii) all the carbonaceous aerosol

133   concentrations are based on IMPROVE-A, except MSOC which did not rely on analytical protocol.

134   The MSOC to OC ratios averaged 0.90 $\pm$0.05, indicating an overall high extraction efficiency of

135   methanol for dissolving organic aerosols.

136   Light absorption spectra of the methanol extracts were measured over the wavelength (λ) range

137   of 200–1110 nm, using a spectrophotometer coupled with a 2.5-m long liquid waveguide capillary

138   cell (LWCC; World Precision Instrument, FL, USA). The spectrophotometer, consisting of a DH-

139   mini UV-VIS-NIR light source and a Maya2000 Pro spectrometer (Ocean Optics Inc., FL, USA),

140   provided wavelength-resolved optical attenuation (ATN_λ) of the dissolved BrC, which could then

141   be converted to BrC absorption coefficient [$(b_{abs})_\lambda$] (Hecobian et al., 2010). The ratio of $(b_{abs})_\lambda$ to

142   MSOC concentration was considered the bulk mass absorption efficiency (MAE_λ) of brown carbon,

143   given the close-to-one MSOC/OC. The wavelength dependence of BrC absorption was determined

144   based on $\ln(ATN_\lambda)$ and $\ln(\lambda)$, and was expressed as the absorption Ångström exponent (AAE). The

145   AAE calculation was performed over 310–460 nm, the same λ range adopted by previous studies

146   conducted at the same site using the same laboratory analysis procedures (Cheng et al., 2022a).

147   **2.3 Additional data sets used**

148   Air quality data and meteorological data were obtained with a time resolution of 1 hour from

149   the China National Environmental Monitoring Center (CNEMC; https://air.cnemc.cn:18007/, last

150   access: 1 January, 2023) and Weather Underground (https://www.wunderground.com/, last access:

151   1 January, 2023), respectively. CNEMC operated 12 monitoring sites in Harbin, with 3 of them

152   located within ~5 km from the HIT sampling site. The reconstructed $PM_{2.5}$ masses, which were

153   derived from observational results on aerosol compositions at HIT, were generally in line with the

154   fine particle concentrations directly measured at the nearby CNEMC sites. Here the reconstructed

155    $PM_{2.5}$ was calculated as the sum of organic matter (1.6 $\times$OC), elemental carbon and inorganic ions.

156   Comparison of the reconstructed and directly-measured $PM_{2.5}$ concentrations showed relative

157   standard deviations of 9–11% (in terms of median value) for the three CNEMC sites nearby,

158   demonstrating HIT as a representative urban site for Harbin. In this study, only the air quality data

159   from the nearest CNEMC site, i.e., Taiping Hongwei Park, were further investigated together with

160   the aerosol components measured at HIT.

161   **3. Results and discussion**

162   **3.1 Why was the wintertime brown carbon more absorbing at night?**

163   The wavelength-resolved b_{abs} and MAE were primarily explored at 365 nm, and the

164   corresponding values were referred to as $(b_{abs})_{365}$ and MAE_{365}, respectively. $(b_{abs})_{365}$ and MSOC

165   correlated strongly for the winter campaign (Figure 1a), that the linear regression of $(b_{abs})_{365}$ against

166   MSOC led to an r value of 0.97 and a slope of 1.63 $\pm$0.02 m^2/gC (with the intercept set as zero;

167   MAE_{365} averaged 1.55 $\pm$0.18 m^2/gC). However, as shown in Figure 1b, the nighttime samples were

168   found to exhibit ~~slightly~~ higher MAE_{365} values (averaging 1.61 $\pm$0.15 m^2/gC) than the daytime ones

169   (averaging 1.48 $\pm$0.18 m^2/gC), with significant differences at the 95% confidence level (2-tailed p

170   = 0.004). ~~with averages of 1.61 $\pm$0.15 and 1.48 $\pm$0.18 m^2/gC, respectively (Figure 1b).~~ In this study,

171   we did not perform source apportionment analysis for brown carbon due to the relatively small

172   number of samples collected. Instead, several indirect indicators were introduced to interpret the

173   diurnal variations of MAE$_{365}$. Statistical results for the comparisons performed in the following

174   discussions are summarized in Table S1.

175   The first indicator was the levoglucosan to OC ratio (LG/OC; on a basis of carbon mass, the

176   same hereinafter). In general, higher LG/OC values indicate a stronger contribution of biomass

177   burning (BB) emissions to OC. The BB activities in January could be attributed primarily to

178   household use of biofuels, e.g., for heating and cooking. This is because (i) few fire hotspot was

179   detected in Harbin and surrounding regions throughout the winter campaign (Figure 2a), and (ii) the

180   relationship between LG and water-soluble potassium (K$^+$), another commonly-used BB tracer, did

181   not show evidence for apparent influence of open burning (Figure 3a). As suggested by previous

182   studies conducted during heating season in Harbin (Cheng et al., 2022b), the LG to K$^+$ ratios were

183   relatively low and constant (~0.5) with the absence of agricultural fires, but became substantially

184   higher (typically above 1.0) during open burning episodes. This pattern was attributed to the

185   relatively low combustion efficiencies (CE) of agricultural fires, which favored the increase of LG

186   emissions but would not change K$^+$ emissions significantly (Gao et al., 2003). It should be noted

187   that in Cheng et al. (2022b), CE were not directly measured for different types of burning activities

188   and instead were investigated based on the ratios of BB organic carbon to BB elemental carbon (R_{BB},

189   derived from positive matrix factorization, i.e., PMF, analysis). Substantial increases of R_{BB} were

190   repeatedly observed during open burning episodes occurring in different seasons, e.g., winter or

191   spring depending on the regulatory policies. Thus the agricultural fires were inferred to have

192   relatively low CE levels compared to residential burning of crop residues (Cheng et al., 2022b), as

193   BB source emission studies typically showed a decreasing trend for the emission ratio of organic

194 carbon to elemental carbon with increasing combustion efficiency (Pokhrel et al., 2016; McClure et

195 al., 2020). Actually, crop residues burned on farmland were usually not intentionally dried and thus

196 could have relatively high water contents. This may partially explain the relatively low CE of

197 agricultural fires. In the present study, LG correlated strongly with K^+ for the entire January (r =

198 0.96, with a slope, i.e., $\Delta LG/\Delta K^+$, of 0.55 $\pm$0.02; Figure 3a) and the LG to K^+ ratios averaged 0.46

199 $\pm$0.11, pointing to the dominance of residential burning in BB emissions. In addition, the residential

200 burning activities were more intensive at night, as can be seen from the elevated LG/OC compared

201 to daytime results (1.10 $\pm$0.26% vs. 0.88 $\pm$0.22%, 2-tailed p = 0.001; Figure 1c). Comparison of

202 the LG to EC ratios between the nighttime and daytime samples (0.22 $\pm$0.06 vs. 0.15 $\pm$0.05, 2-

203 tailed p = 0.000) reached the same conclusion. Indeed, biomass burning could emit a number of

204 strong chromophores such as nitrogen-containing aromatic compounds (Mohr et al., 2013; Lin et

205 al., 2016, 2017; Xie et al., 2019; Salvador et al., 2021). However, for the January samples, MAE_{365}

206 did not show clear dependence on LG/OC or LG/EC (r = 0.42 and 0.12, respectively; Figure 1e),

207 suggesting that in addition to BB emissions, there must exist other factors that were more

208 responsible for the diurnal variations of wintertime MAE_{365}.

209   The second indicator was $R_{S/N}$, defined as the ratio of (n-sulfur dioxide + n-sulfate) to (n-

210 nitrogen dioxide + n-nitrate), where "n" indicates molar concentration. Given that sulfate and nitrate

211 are typically considered as secondary, $R_{S/N}$ could be roughly traced back to the emission ratios of

212 sulfur dioxide (SO_2) to nitrogen oxides (NO_x), i.e., $E_{S/N}$, from combustion of various types of fuels

213 (e.g., coal, gasoline, diesel and biomass). Previous studies suggested that $E_{S/N}$ differed substantially

214 between emissions from vehicles, coal combustion and biomass burning. In China, the fuel quality

215 standards have been greatly strengthened for on-road vehicles since early 2000s, e.g., the maximum

216   sulfur content allowed in diesel was reduced from 2000 ppm (required by the China I standard

217   implemented in 2002) to 10 ppm (required by the China V standard implemented in 2017). Thus,

218   recent studies on vehicular exhausts typically suggested that the SO_2 emission factors (EF-SO_2)

219   were about two orders of magnitude lower than those of NOx (EF-NOx; Zhang et al., 2015; Li et

220   al., 2019) and consequently, the corresponding $E_{S/N}$ should be approximately $\sim10^{-2}$. EF-SO_2 were

221   also usually lower than EF-NOx for biomass burning (Zhang et al., 2000; McMeeking et al., 2009;

222   Liu et al., 2016; Wu et al., 2022), but their differences were not as large as those observed in vehicle

223   emissions, leading to $E_{S/N}$ values of $\sim10^{-1}$. Unlike vehicles or biomass burning, coal combustion

224   usually resulted in higher EF-SO_2 compared to EF-NOx (Zhang et al., 2000; Du et al., 2017; Li et

225   al., 2017), which could be translated to $E_{S/N}$ values of above one. On the other hand, primary species

226   could be transformed rapidly during atmospheric aging, e.g., a sharp loss of NO_x and a

227   corresponding burst in nitrate were observed shortly after emission when tracking plumes from

228   diesel trucks (Shen et al., 2021) and agricultural fires (Akagi et al., 2012; Liu et al., 2016). Thus it

229   should be acceptable to assume that for the pollutants emitted by a specific source, the $R_{S/N}$ of aged

230   plumes was generally comparable with the $E_{S/N}$ of fresh emissions.

231   The ambient $R_{S/N}$ averaged 0.6 ± 0.2 during the winter campaign, differing substantially from

232   the $E_{S/N}$ of coal combustion or vehicle emissions but in the same order of magnitude as the $E_{S/N}$ of

233   biomass burning. Actually, no evidence supported BB emissions as a major regulating factor for

234    $R_{S/N}$, e.g., as indicated by the insignificant correlations between $R_{S/N}$ and LG/EC ($r = 0.24$ and 0.01

235   for the daytime and nighttime samples, respectively). Then $R_{S/N}$ was expected to be more sensitive

236   to the changes of coal combustion and vehicle emissions, e.g., increase of coal combustion

237   emissions would effectively elevate $R_{S/N}$ whereas higher vehicle emissions favor the decrease of

$R_{S/N}$. During the winter campaign, lower $R_{S/N}$ were observed at night (Figure 1d), averaging 0.5 $\pm$ 0.1 compared to an average $R_{S/N}$ of 0.7 $\pm$ 0.2 for the daytime samples (2-tailed p = 0.000). In principle, this pattern could be caused by decreased coal combustion emissions and/or increased vehicle emissions at night. However, it seemed that the former did not play an important role, since many coal combustion activities (e.g., those for heating supply, power generation and some industrial processes) were uninterruptible, i.e., would not be stopped at night (Lian et al., 2020; Chu et al., 2021; Yuan et al., 2021). Then the most likely cause for the lower nighttime $R_{S/N}$ was increased vehicle emissions. According to the Road Traffic Regulations released by Harbin, heavy-duty diesel trucks (HDDT), which are known to include high- or super-emitters (Dallmann et al., 2012), are allowed to run on the roads in the main urban area only from 21:00 to 5:00 of the next day. This to a large extent explains the inference on the increase of vehicle emissions during nighttime. MAE$_{365}$ exhibited a clear negative dependence on $R_{S/N}$ for all the winter samples (Figure 1f), suggesting vehicle emissions, especially those from HDDT, as a dominant influencing factor for MAE$_{365}$ (under the precondition of relatively stable coal combustion emissions).

The last two indicators were associated with secondary aerosol formation, including the sulfur oxidation ratio (SOR) and the nitrogen oxidation ratio (NOR) defined as n-sulfate/(n-sulfate + n-SO$_2$) and n-nitrate/(n-nitrate + n-NO$_2$), respectively. The entire winter campaign experienced low temperatures, which averaged -16 ± 5 and -21 ± 6 °C for the daytime and nighttime samples, respectively. In general, the transformation of gaseous precursors to secondary inorganic ions was inefficient in the frigid atmosphere, as indicated by the overall low levels of both SOR and NOR. However, both indicators exhibited noticeable differences between daytime and nighttime samples. The diurnal variation of SOR was found to be associated with the higher relative humidity (RH)

260 levels at night (Figure 4a). For the vast majority of winter samples, RH fell into the ranges of 60–

261 80 and 70–90% during daytime and nighttime, respectively. SOR were largely unchanged when RH

262 increased from 60–70% to 70–80% during the day, whereas for the common RH range shared by

263 the daytime and nighttime samples (i.e., 70–80%), SOR ~~were slightly~~ tended to be slightly lower at

264 night, likely due to the drop of temperatures. In addition, a positive dependence of SOR on RH was

265 evident for the nighttime samples. Although SOR showed almost the same median values (~0.1) for

266 the RH ranges of 70–80 and 80–90% at night, relatively high SOR levels of above 0.2 were more

267 frequently observed in the latter case. Such high SOR were rarely seen during the day, indicating

268 that RH played a more important role than temperature in sulfate formation. The enhanced sulfate

269 formation at high RH was presumably through heterogeneous reactions (Su et al., 2020; Liu et al.,

270 2021), since the low temperatures encountered during the winter campaign did not rule out the

271 presence of aerosol water, e.g., liquid water was observed to remain super-cooled in clouds down to

272 temperatures of as low as –40 °C (Tabazadeh et al., 2002). Compared to SOR, different patterns of

273 diurnal variation were observed for NOR (Figure 4b). First, the difference between daytime and

274 nighttime NOR was more significant for the RH range of 70–80%, e.g., as indicated by the larger

275 decrease of median NOR at night (0.06, compared to a corresponding value of 0.02 for SOR).

276 Second, the nighttime NOR elevated substantially as RH increased from 70–80% to 80–90%, but

277 still with lower levels compared to the daytime results. Given that relatively low temperatures favor

278 the partitioning of semi-volatile nitrate into aerosol phase, the less efficient nitrate formation at night

279 could not be explained by the partitioning process and instead should be primarily attributed to

280 reduced photooxidation of NO_2 (Chen et al., 2020). Based on a synthesis of the diurnal variations

281 observed for SOR and NOR, the nighttime samples were characterized by enhanced heterogeneous

chemistry, which did not require sunlight as indicated by the RH-dependent increase of SOR under

dark conditions, and weakened photochemical reactions. The overall effect of these two factors on

secondary organic aerosol (SOA) formation was inconclusive and thus it remained difficult to

robustly unfold the role of SOA in the diurnal variations of MAE_{365}. Actually, it appeared that

MAE_{365} was not strongly influenced by SOA during the winter campaign. For example, when RH

increased from 70–80% to 80–90% at night, the MAE_{365} were nearly constant (e.g., with the same

average value of 1.6 m^2/gC for the two RH ranges) despite the enhancement of heterogeneous

chemistry.

3.2 Why did the springtime MAE_{365} show more significant diurnal variations?

Compared to the wintertime results, the average MAE_{365} was lower in spring (1.33 vs. 1.55

m^2/gC) but the corresponding standard deviation was much higher (0.62 vs. 0.18 m^2/gC), indicating

that the spring samples varied more significantly with respect to the absorption capacity of brown

carbon (Figure 5a). This feature could also be seen from the more pronounced diurnal variations of

MAE_{365} observed in spring (Figure 5b), e.g., the nighttime MAE_{365} were on average ~70% (2-tailed

$p = 0.000$) and 10% (2-tailed $p = 0.004$) larger than the daytime values during the spring and winter

measurement periods, respectively. For the winter campaign, the slightly elevated MAE_{365} at night

had been primarily attributed to increased vehicle emissions, as indicated by a ~35% decrease of

$R_{S/N}$. In spring, $R_{S/N}$ were also lower at night (2-tailed $p = 0.000$), by ~40% compared to the daytime

results (Figure 5d). Given that the two campaigns showed comparable discrepancies between the

nighttime and daytime $R_{S/N}$, increase of vehicle emissions at night was presumably not the dominant

driver for the much stronger diurnal variations of MAE_{365} observed in spring. Actually, MAE_{365} was

almost independent of $R_{S/N}$ for the spring samples. For example, the MAE_{365} values were found to

304   fall into two well-separated ranges (above 2 and ~0.5–1.5 m^2/gC, with the former observed only at

305   night) for the samples with relatively low $R_{S/N}$ levels (below 0.4), indicating that reduced $R_{S/N}$ was

306   ineffective to explain the high MAE_{365} events encountered in spring (Figure 5f). In addition to

307   increased vehicle emissions at night, therefore, there must exist other factors which were more

308   responsible for the significant diurnal variations of springtime MAE_{365}.

309   We first evaluated the influence of secondary aerosol formation. The spring campaign

310   experienced lower RH and substantially higher temperatures compared to winter, by ~25% and

311   30 ℃, respectively. The springtime SOR ~~were~~ appeared to be slightly lower than the wintertime

312   results (0.12 ± 0.06 vs. 0.15 ± 0.07), whereas an opposite pattern was observed for NOR (0.16 ±

313   0.08 vs. 0.12 ± 0.06). The seasonal variations of SOR and NOR provided additional evidence for

314   the inferences that the sulfate and nitrate formation was more strongly contributed by heterogeneous

315   and photochemical reactions, respectively. For the spring campaign, the daytime and nighttime SOR

316   were in general comparable (Figure S1a) and no clear evidence was observed for the prevalence of

317   heterogeneous chemistry, presumably due to the rare occurrence of high RH conditions either during

318   the day or at night. Unlike SOR, the daytime NOR ~~were considerably~~ tended to be slightly higher

319   than the nighttime results (0.18 ± 0.09 vs. 0.14 ± 0.08; Figure S1b), pointing to enhanced

320   photochemistry during the day. This pattern could be partially responsible for the relatively low

321   daytime MAE_{365}, since secondary brown carbon was typically less light-absorbing than primary

322   BrC (Kumar et al., 2018; Cappa et al., 2020; Ni et al., 2021). However, MAE_{365} did not exhibit clear

323   dependence on NOR or the nitrate to OC ratio (NO_3^-/OC), e.g., the high MAE_{365} events were found

324   to be associated with moderate NOR and NO_3^-/OC levels (Figure S2). Thus for the spring campaign,

325   photochemistry should not be the major influencing factor for MAE_{365}, either.

326   We then investigated the role of biomass burning. Unlike the wintertime results, MAE_{365}

327   showed a strong positive correlation with LG/OC ($r = 0.84$) in spring (Figure 5e), suggesting

328   biomass burning emissions as the dominant driver for the variations of MAE_{365}. It is noteworthy

329   that the LG to OC ratios were substantially higher in spring than in winter (2-tailed $p = 0.000$), with

330   averages of $3.11 \pm 1.70\%$ and $0.99 \pm 0.26\%$, respectively. This pattern could not be explained by

331   seasonal variations in residential consumption of biofuels, since April experienced much higher

332   temperatures than January (averaging 11 and -19 °C, respectively). Instead, the elevated springtime

333   LG/OC should be attributed primarily to open burning, as supported by the intensive fire hotspots

334   detected around Harbin in April (Figure 2b). The seasonal variations of LG to K^+ ratio (LG/K^+) also

335   suggested that the dominant burning ways were different between winter and spring. Compared to

336   the relatively small and constant LG/K^+ observed in January (0.46 ± 0.11), the ratios were nearly

337   tripled in April (1.28 ± 0.61) with more significant sample-by-sample differences (between ~0.5–

338   3.5) (Figure 3b). Recalling that the transition from flaming to smoldering combustion favored the

339   increase of LG/K^+ (Gao et al., 2003), the springtime burning should have relatively low and variable

340   combustion efficiencies. This inference was in line with the fact that the agricultural fires were

341   usually uncontrolled, e.g., with respect to water content of crop residues and abundance of oxygen.

342   In all, for the spring campaign, the dominant driver for the variations of LG/OC and MAE_{365} could

343   be further identified as open burning. Subsequently, the higher LG/OC and MAE_{365} at night (Figures

344   5b–5c) could be attributed primarily to increased agricultural fires. The preference on nighttime

345   burning was not surprising, since the agricultural fires were illegal, i.e., nominally prohibited by the

346   Government of Heilongjiang Province.

347   It should be noted that the agricultural fire emissions increased LG/OC but had minimal

348 influence on $R_{S/N}$ (Figure S3). For example, the nighttime samples collected in spring differed

349 substantially with respect to the impact of agricultural fires, as indicated by their variable LG/OC

350 which spanned nearly one order of magnitude. However, no clear pattern was observed for $R_{S/N}$ with

351 increasing LG/OC, e.g., linear regression of $R_{S/N}$ on LG/OC showed an extremely low r value of

352 0.07.

353   The frequent occurrences of agricultural fires during April, 2021 to some extent masked the

354 "background" MAE_{365}, i.e., the value representative for the spring conditions without significant

355 influence of open burning. In spring, all the samples with LG/K^+ ratios of above one, i.e., a chemical

356 signature for apparent impacts of agricultural fires, were found to have LG/OC ratios larger than

357 2%. In addition, LG/OC ratio could also work as an estimate of the strength of biomass burning

358 impact. Thus in the following discussions, LG/OC of $>$ 2% was used as an indicator for open burning

359 episodes and correspondingly, spring samples with LG/OC of below 2% were referred to as typical

360 ones. MAE_{365} averaged 0.80 $\pm$0.22 m^2/gC for the typical samples of spring, lower than results from

361 the winter campaign (1.55 $\pm$ 0.18 m^2/gC; Figure S4a). This seasonal pattern coincided with the

362 overall lower $R_{S/N}$ in spring (Figure S4b). It was unlikely that the number of in-use vehicles or the

363 fleet composition in Harbin could vary significantly between January and April of the same year.

364 Thus the reduced springtime $R_{S/N}$, i.e., the relatively low MAE_{365} with the absence of agricultural

365 fires, should be caused mainly by the decrease of coal combustion emissions, e.g., due to the less

366 demand for heating.

367 **3.3 Unique wavelength dependence of BrC absorption during agricultural fire episodes**

368   The agricultural fires not only elevated MAE_{365} but also changed the wavelength dependence

369 of brown carbon. For the wavelength range used for AAE calculation (310–460 nm), the detection

370   limit of optical attenuation (ATN_{LOD}) was ~0.02, which was determined as three times the maximum

371   standard deviation of parallel ATN_λ results from blank filters. Before further discussions, we

372   introduced a new term "relative $ln(ATN_\lambda)$", i.e., $ln(ATN_\lambda)^*$ calculated as $ln(ATN_\lambda) - ln(ATN_{LOD})$. A

373   benefit of using the new term was that a $ln(ATN_\lambda)^*$ value of zero corresponded to $ATN_\lambda = ATN_{LOD}$

374   and thus $ln(ATN_\lambda)^*$ could be considered "real" absorption by chromophores in solutions.

375   ~~corresponded to ATN_{LOD} and thus could be interpreted independently, e.g., ATN_{LOD} was~~

376   ~~independent of the sampling or analytical procedures such as the volume of methanol used for~~

377   ~~extraction.~~ It should be noted that the use of $ln(ATN_\lambda)^*$ would not influence the determination of

378   AAE, since the same slope would be derived from the regressions of $ln(ATN_\lambda)^*$ and $ln(ATN_\lambda)$ on

379   $ln(\lambda)$. For the typical samples of spring, the dependence of $ln(ATN_\lambda)^*$ on $ln(\lambda)$ could be properly

380   approximated by a linear function, usually with *r* values of above 0.995. In this case, AAE could be

381   reliably determined, and an average value of 6.92 ±0.28 was obtained.

382   The relationship between $ln(ATN_\lambda)^*$ and $ln(\lambda)$ became non-linear for the open burning episodes.

383   To more quantitatively describe the non-linearity, we added an "auxiliary line" to each measured

384   spectrum (Figure 6a), by drawing a line between the two points with *x* values of $ln(310)$ and $ln(460)$.

385   The "auxiliary line" could be considered an assumed spectrum with linear dependence of $ln(ATN_\lambda)^*$

386   on $ln(\lambda)$. The measured spectrum was always above the assumed one and their largest difference

387   was typically observed at ~365 nm, pointing to the presence of distinct BrC chromophores with

388   absorption peak around this wavelength.

389   The influence of such chromophores on BrC absorption could be estimated by the following

390   three indicators. The first one (*F*) was related to the difference between the measured and assumed

391   $ln(ATN_\lambda)^*$ at 365 nm:

$$F = \left[\ln\left(\mathrm{ATN}_{365}\right)_{\mathrm{m}}^{*} - \ln\left(\mathrm{ATN}_{365}\right)_{\mathrm{a}}^{*} \right] \Big/ \ln\left(\mathrm{ATN}_{365}\right)_{\mathrm{a}}^{*}$$, where the subscripts "m" and "a" indicate

results from the measured and assumed spectra, respectively (Figure 6a). The second indicator (K)

was related to the area enclosed between the two spectra (S_2): $K = S_2/S_1$, where S_1 indicates the area

enclosed by the assumed spectrum and x-axis (Figure 6b). The last indicator was $\Delta(b_{\mathrm{abs}})_{365}$

calculated as $\left(b_{\mathrm{abs}}\right)_{365}^{\mathrm{m}} - \left(b_{\mathrm{abs}}\right)_{365}^{\mathrm{a}}$, where the superscripts "m" and "a" indicate absorption

coefficients calculated based on the measured and assumed spectra, respectively. F and K exhibited

a strong linear correlation for the open burning episodes ($r = 0.99$; Figure 6c), indicating that the

differences between the measured and assumed spectra were likely caused by the same class of BrC

compounds. In addition, these compounds could be primarily traced back to biomass burning, since

$\Delta(b_{\mathrm{abs}})_{365}$ showed a positive dependence on LG/OC (Figure 6d). ~~A candidate for such compounds~~

~~was C₇H₇NO₄ (a methyl-substituted nitrocatechol),~~ Candidates for such compounds were aromatic

species with nitro-functional groups, based on a synthesis of absorption spectra measured for

various BrC chromophores (Huang et al., 2020) and molecular characterization results for biomass

burning emissions (Lin et al., 2016, 2017; Xie et al., 2019, 2020). Chamber experiments by Iinuma

et al. (2010) suggested that ~~C₇H₇NO₄~~ aromatic compounds with nitro-functional groups could also

be formed through photooxidation of gaseous precursors emitted by biomass burning (m-cresol). In

this study, however, all the samples with relatively high $\Delta(b_{\mathrm{abs}})_{365}$ levels (e.g., above 20 Mm^{-1}) were

collected at night, indicating that the distinct BrC chromophores with absorption peak at ~365 nm

~~(like C₇H₇NO₄)~~ were more strongly associated with primary emissions from agricultural fires. In

addition, the chromophores seemed to be subject to photo-bleaching, as both F and K decreased

substantially (by ~65%) during the day compared to the nighttime results (Figure 7).

For the open burning episodes, the distinct absorption peak at ~365 nm prohibited a proper

414   determination of AAE. If enforcing a linear function for the dependence of $\ln(ATN_\lambda)^*$ on $\ln(\lambda)$, lower

415   r values would be derived (down to ~0.97, with an average of 0.992 ±0.007) compared to the typical

416   samples (averaging 0.998 ±0.002). In addition, r showed a decreasing trends with the increases of

417   LG/OC (Figure 6e) and F (Figure S5), suggesting that the relationship between $\ln(ATN_\lambda)^*$ and $\ln(\lambda)$

418   deviated more significantly from linearity as the ~365 nm absorption peak, i.e., the influence of

419   agricultural fires, became more significant. We suggest that for the open burning episodes, the AAE

420   results should be interpreted with caution, although they could be calculated mathematically with

421   reasonable r values (e.g., even the minimum r appeared acceptable).

422   **3.4 Diurnal variations of wintertime AAE**

423   Similar to the typical samples of spring, $\ln(ATN_\lambda)^*$ exhibited linear dependences on $\ln(\lambda)$ for

424   all the winter samples. The wintertime AAE were higher at night compared to those observed during

425   the day (with averages of 7.33 ±0.14 and 6.76 ±0.11, respectively; 2-tailed $p = 0.000$), consistent

426   with the pattern observed during winter in Beijing (Li et al., 2020). The relative abundance of

427   secondary OC (SOC) has been considered an important influencing factor for AAE, e.g., an

428   increasing trend was observed for AAE during long-range transport of BrC over the Indo-Gangetic

429   Plain (Dasari et al., 2019). Although SOC or its organic tracer was not determined in this study,

430   previous source apportionment results from Harbin (based on PMF) showed a strong correlation

431   between SOC and sulfate, with largely consistent relationships among different campaigns (Cheng

432   et al., 2022b). Thus we used sulfate as an indicator for SOC. During the winter campaign, the sulfate

433   to OC ratios were lower at night (averaging 0.38, compared to 0.44 during the day; 2-tailed $p =$

434   0.011), pointing to decreased fractions of SOC in OC. This inference was consistent with the higher

435   LG/OC and $R_{S/N}$ levels observed at night, which had been attributed to increased emissions from

436   residential biomass burning and vehicular exhausts, respectively. Thus regarding the association

437   between AAE and SOC formation, results from the winter campaign were inconsistent with Dasari

438   et al. (2019), but the reason remained unclear. Molecular characterization of organic aerosols should

439   be necessary to unfold the response of AAE to changes in BrC sources.

440   **4. Conclusions**

441   Diurnal variations of BrC were investigated during two distinct seasons in the northernmost

442   megacity in China. The winter campaign was characterized by low temperatures rarely seen in other

443   hotspots of air pollution studies such as the North China Plain. The wintertime BrC aerosols were

444   slightly more absorbing at night, with an average MAE_{365} of 1.61 $\pm$0.15 m^2/gC compared to 1.48 $\pm$

445   0.18 m^2/gC during the day. Various indicators were used to explain the observed diurnal variations

446   of MAE_{365}, including those associated with biomass burning emissions (LG/K$^+$ and LG/OC),

447   relative importance of coal combustion and vehicle emissions ($R_{S/N}$) and secondary aerosol

448   formation (SOR and NOR). For the winter campaign, the nighttime samples were characterized by

449   increased BB emissions from residential sources, enhanced heterogeneous chemistry and weakened

450   photochemical reactions. But none of these factors was identified as the dominant driver for the

451   higher MAE_{365} at night. Instead, MAE_{365} exhibited a negative dependence on $R_{S/N}$, and the lower

452   $R_{S/N}$ and thus higher MAE_{365} at night were primarily attributed to increased emissions from heavy-

453   duty diesel trucks, which were not allowed in the main urban area during the day. In addition, the

454   wintertime AAE were higher at night but it remained difficult to unfold the underlying connection

455   between this diurnal pattern and the changes in BrC sources.

456   The spring campaign was characterized by frequent occurrences of agricultural fires, with more

457   pronounced diurnal variations of MAE_{365} (averaging 0.98 $\pm$ 0.31 and 1.69 $\pm$ 0.65 m^2/gC for the

458 daytime and nighttime samples, respectively). Unlike winter, the springtime MAE_{365} were mainly

459 influenced by open burning emissions, as suggested by the positive dependence of MAE_{365} on

460 LG/OC and the lack of correlation between MAE_{365} and $R_{S/N}$. The higher nighttime LG/OC

461 indicated that the farmers preferred burning the crop residues at night, presumably because

462 agricultural fires were nominally prohibited by the local government. In addition, BrC exhibited

463 distinct light absorption spectra during agricultural fire episodes, as indicated by the non-linear

464 relationship between $\ln(ATN_\lambda)^*$ on $\ln(\lambda)$. The non-linearity was mainly caused by chromophores

465 with absorption peak at ~365 nm, which became more significant with increasing BB influence. A

466 candidate for the compounds at play was $C_7H_7NO_4$, based on a synthesis of absorption spectra

467 measured for various BrC chromophores and molecular measurement results for BB emissions.

468 Aromatic species with nitro-functional groups were a possible class of compounds that were at play.

469 The presence of such chromophores, i.e., the distinct absorption peak at ~365 nm, prohibited a

470 proper determination of AAE for the spring samples impacted by agricultural fires.

471 **5. Implications**

472   MAE_{365} and AAE are key parameters for simulating climate effects of brown carbon. In winter,

473 although Harbin experiences low temperatures rarely seen in other Chinese megacities, the observed

474 MAE_{365} and AAE were largely comparable with the typical results from other regions in Northern

475 China (e.g., Beijing; Cheng et al., 2016). In addition, BrC's optical properties were indeed different

476 between daytime and nighttime samples, which were likely associated with increased HDDT

477 emissions at night. However, the diurnal variations (~10% higher at night for both MAE_{365} and AAE)

478 appeared negligible compared to uncertainties in simulating the mass concentration of BrC, i.e.,

479 organic aerosol. Thus for typical winter conditions in Northern China (without open burning), it

may be practical to use fixed MAE_{365} and AAE values for estimating the wavelength-resolved absorption by organic aerosol in climate models.

The spring campaign suggested another scenario, that the agricultural fires exhibited strong influences on optical properties of brown carbon, as highlighted by the ~365 nm peak in BrC's absorption spectra. The distinct peak on one hand effectively elevated MAE_{365}, and on the other hand complicated the determination of AAE. In addition, the peak became less significant during the day, indicating that the organic compounds at play were likely subject to photo-bleaching. BrC emitted by the fires remained difficult to constrain, partially due to the variable combustion efficiencies. This in turn resulted in challenges for simulating climate effects of the open burning aerosols. Given the massive agricultural sector in Northeast China, more studies are necessary to understand the emissions, transformation and impacts of the fire-induced pollutants.

Data availability. Data described in this manuscript can be accessed at https://doi.org/10.5281/zenodo.7874760 (Cheng, 2023).

Author contributions. YC and JL designed the study and prepared the paper with inputs from all the co-authors. XC, YZ and QY carried out the experiments. QZ and KH validated the results and supervised the study.

Competing interests. Author Qiang Zhang is a member of the editorial board of *Atmospheric Chemistry and Physics*. The peer-review process was guided by an independent editor, and the authors have also no other competing interests to declare.

Acknowledgements. The authors thank Zhen-yu Du at National Research Center for Environmental Analysis and Measurement, and Lin-lin Liang at Chinese Academy of Meteorological Sciences for their help in sample analysis.

Financial support. This research has been supported by the National Natural Science Foundation

of China (42222706), the Natural Science Foundation of Heilongjiang Province (LH2020D011),

Fundamental Research Funds for the Central Universities, and Heilongjiang Touyan Team.

References

Akagi, S. K., Craven, J. S., Taylor, J. W., McMeeking, G. R., Yokelson, R. J., Burling, I. R., Urbanski,
S. P., Wold, C. E., Seinfeld, J. H., Coe, H., Alvarado, M. J., and Weise, D. R.: Evolution of
trace gases and particles emitted by a chaparral fire in California, *Atmos. Chem. Phys.*, 12,
1397–1421, https://doi.org/10.5194/acp-12-1397-2012, 2012.

Brege, M. A., China, S., Schum, S., Zelenyuk, A., and Mazzoleni, L. R.: Extreme molecular
complexity resulting in a continuum of carbonaceous species in biomass burning tar balls from
wildfire smoke, *ACS Earth Space Chem.*, 5, 2729–2739,
https://doi.org/10.1021/acsearthspacechem.1c00141, 2015.

Brown, H., Liu, X. H., Feng, Y., Jiang, Y. Q., Wu, M. X., Lu, Z., Wu, C. L., Murphy, S., and Pokhrel,
R.: Radiative effect and climate impacts of brown carbon with the Community Atmosphere
Model (CAM5), *Atmos. Chem. Phys.*, 18, 17745–17768, https://doi.org/10.5194/acp-18-
17745-2018, 2018.

Cappa, C. D., Lim, C. Y., Hagan, D. H., Coggon, M., Koss, A., Sekimoto, K., de Gouw, J., Onasch,
T. B., Warneke, C., and Kroll, J. H.: Biomass-burning-derived particles from a wide variety of
fuels – Part 2: effects of photochemical aging on particle optical and chemical properties,
Atmos. Chem. Phys., 20, 8511–8532, https://doi.org/10.5194/acp-20-8511-2020, 2020.

Chen, X. R., Wang, H. C., Lu, K. D., Li, C. M., Zhai, T. Y., Tan, Z. F., Ma, X. F., Yang, X. P., Liu,
Y. H., Chen, S. Y., Dong, H. B., Li, X., Wu, Z. J., Hu, M., Zeng, L. M., and Zhang, Y. H.: Field
determination of nitrate formation pathway in winter Beijing, *Environ. Sci. Technol.*, 54,
9243–9253, https://doi.org/10.1021/acs.est.0c00972, 2020.

Chen, Y., and Bond, T. C.: Light absorption by organic carbon from wood combustion, *Atmos.
Chem. Phys.*, 10, 1773–1787, https://doi.org/10.5194/acp-10-1773-2010, 2010.

Cheng, Y.: Diurnal variations of brown carbon during two distinct seasons in a megacity in
Northeast China [data set], https://doi.org/10.5281/zenodo.7874760, 2023.

Cheng, Y., He, K. B., Du, Z. Y., Engling, G., Liu, J. M., Ma, Y. L., Zheng, M., and Weber, R. J.: The
characteristics of brown carbon aerosol during winter in Beijing, *Atmos. Environ.*, 127, 355–
364, https://doi.org/10.1016/j.atmosenv.2015.12.035, 2016.

533 Cheng, Y., Cao, X. B., Liu, J. M., Yu, Q. Q., Wang, P., Yan, C. Q., Du, Z. Y., Liang, L. L., Zhang,
534   Q., and He, K. B.: Primary nature of brown carbon absorption in a frigid atmosphere with
535   strong haze chemistry, Environ. Res., 204, 112324,
536   https://doi.org/10.1016/j.envres.2021.112324, 2022a.

537 Cheng, Y., Cao, X. B., Liu, J. M., Yu, Q. Q., Zhong, Y. J., Geng, G. N., Zhang, Q., and He, K. B.:
538   New open burning policy reshaped the aerosol characteristics of agricultural fire episodes in
539   Northeast China, *Sci. Total Environ.*, 810, 152272,
540   https://doi.org/10.1016/j.scitotenv.2021.152272, 2022b.

541 Chu, B. W., Zhang, S. P., Liu, J., Ma, Q. X., and He, H.: Significant concurrent decrease in $PM_{2.5}$
542   and NO_2 concentrations in China during COVID-19 epidemic, *J. Environ. Sci.*, 99, 346–353,
543   https://doi.org/10.1016/j.jes.2020.06.031, 2021.

544 Dallmann, T. R., DeMartini, S. J., Kirchstetter, T. W., Herndon, S. C., Onasch, T. B., Wood, E. C.,
545   and Harley, R. A.: On-road measurement of gas and particle phase pollutant emission factors
546   for individual heavy-duty diesel trucks, *Environ. Sci. Technol.*, 46, 8511–8518,
547   https://doi.org/10.1021/es301936c, 2012.

548 Dasari, S., Andersson, A., Bikkina, S., Holmstrand, H., Budhavant, K., Satheesh, S., Asmi, E., Kesti,
549   J., Backman, J., Salam, A., Bisht, D. S., Tiwari, S., Hameed, Z., and Gustafsson, Ö.:
550   Photochemical degradation affects the light absorption of water-soluble brown carbon in the
551   South Asian outflow, *Sci. Adv.*, 5, eaau8066, https://doi.org/10.1126/sciadv.aau8066, 2019.

552 Du, W., Shen, G. F., Chen, Y. C., Zhu, X., Zhuo, S. J., Zhong, Q. R., Qi, M., Xue, C. Y., Liu, G. Q.,
553   Zeng, E., Xing, B. S., and Tao, S.: Comparison of air pollutant emissions and household air
554   quality in rural homes using improved wood and coal stoves, *Atmos. Environ.*, 166, 215–223,
555   https://doi.org/10.1016/j.atmosenv.2017.07.029, 2017.

556 Engling, G., Carrico, C. M., Kreidenweis, S. M., Collett Jr., J. L., Day, D. E., Malm, W. C., Lincoln,
557   L., Hao, W. M., Iinuma, Y., and Herrmann, H.: Determination of levoglucosan in biomass
558   combustion aerosol by high-performance anion-exchange chromatography with pulsed
559   amperometric detection, *Atmos. Environ.*, 40, S299–S311,
560   https://doi.org/10.1016/j.atmosenv.2005.12.069, 2006.

561 Gao, S., Hegg, D. A., Hobbs, P. V., Kirchstetter, T. W., Magi, B. I., and Sadilek, M.: Water-soluble
562   organic components in aerosols associated with savanna fires in southern Africa: identification,
563   evolution, and distribution, *J. Geophys. Res.*, 108, D13, 8491,
564   https://doi.org/10.1029/2002JD002324, 2003.

565 Hecobian, A., Zhang, X., Zheng, M., Frank, N., Edgerton, E. S., and Weber, R. J.: Water-soluble
566   organic aerosol material and the light-absorption characteristics of aqueous extracts measured

567 over the Southeastern United States, *Atmos. Chem. Phys.*, 10, 5965–5977,
568 https://doi.org/10.5194/acp-10-5965-2010, 2010.

569 Huang, R. J., Yang, L., Shen, J .C., Yuan, W., Gong, Y. Q., Guo, J., Cao, W. J., Duan, J., Ni, H. Y.,
570 Zhu, C. S., Dai, W. T., Li, Y. J., Chen, Y., Chen, Q., Wu, Y. F., Zhang, R. J., Dusek, U., and
571 O'Dowd, C.: Water-Insoluble organics dominate brown carbon in wintertime urban aerosol of
572 China: chemical characteristics and optical properties, *Environ. Sci. Technol.*, 54, 7836–7847,
573 https://doi.org/10.1021/acs.est.0c01149, 2020.

574 Huang, R. J., Yang, L., Shen, J. C., Yuan, W., Gong, Y. Q., Ni, H. Y., Duan, J., Yan, J., Huang, H.
575 B., You, Q. H., and Li, Y. J.: Chromophoric fingerprinting of brown carbon from residential
576 biomass burning, *Environ. Sci. Technol. Lett.*, 9, 102–111,
577 https://doi.org/10.1021/acs.estlett.1c00837, 2022.

578 Huo, Y. Q., Guo, Z. H., Li, Q., Wu, D., Ding, X., Liu, A. L., Huang, D., Qiu, G. K., Wu, M. M.,
579 Zhao, Z. J., Sun, H., Song, W. H., Li, X., Chen, Y. J., Wu, T. C., and Chen, J. M.: Chemical
580 fingerprinting of HULIS in particulate matters emitted from residential coal and biomass
581 combustion, *Environ. Sci. Technol.*, 55, 3593–3603,
582 https://doi.org/10.1021/acs.est.0c08518, 2021.

583 Iinuma, Y., Böge, O., Gräfe, R., and Herrmann, H.: Methyl-nitrocatechols: atmospheric tracer
584 compounds for biomass burning secondary organic aerosols, *Environ. Sci. Technol.*, 44, 8453–
585 8459, https://doi.org/10.1021/es102938a, 2010.

586 Jiang, H. X., Li, J., Sun, R., Tian, C. G., Tang, J., Jiang, B., Liao, Y. H., Chen, C. E., and Zhang, G.:
587 Molecular dynamics and light absorption properties of atmospheric dissolved organic matter,
588 *Environ. Sci. Technol.*, 55, 10268–10279, https://doi.org/10.1021/acs.est.1c01770, 2021.

589 Kumar, N. K., Corbin, J. C., Bruns, E. A., Massabó, D., Slowik, J. G., Drinovec, L., Močnik, G.,
590 Prati, P., Vlachou, A., Baltensperger, U., Gysel, M., El-Haddad, I., and Prévôt, A. S. H.:
591 Production of particulate brown carbon during atmospheric aging of residential wood-burning
592 emissions, *Atmos. Chem. Phys.*, 18, 17843–17861, https://doi.org/10.5194/acp-18-17843-
593 2018, 2018.

594 Lack, D. A., Langridge, J. M., Bahreini, R., Cappa, C. D., Middlebrook, A. M., and Schwarz, J. P.:
595 Brown carbon and internal mixing in biomass burning particles, *Proc. Natl. Acad. Sci. USA*,
596 109, 14802–14807, https://doi.org/10.1073/pnas.1206575109, 2012.

597 Laskin, A., Laskin, J., and Nizkorodov, S. A.: Chemistry of atmospheric brown carbon, *Chem. Rev.*,
598 115, 4335–4382, https://doi.org/10.1021/cr5006167, 2015.

599 Li, M., Liu, H., Geng, G. N., Hong, C. P., Liu, F., Song, Y., Tong, D., Zheng, B., Cui, H. Y., Man,

600   H. Y., Zhang, Q., and He, K. B.: Anthropogenic emission inventories in China: a review, *Natl.*
601   *Sci. Rev.*, 4, 834–866, https://doi.org/10.1093/nsr/nwx150, 2017.

602   Li, X., Wang, Y. J., Hu, M., Tan, T. Y., Li, M. R., Wu, Z. J., Chen, S. Y., and Tang, X. Y.:
603   Characterizing chemical composition and light absorption of nitroaromatic compounds in the
604   winter of Beijing, *Atmos. Environ.*, 237, 117712,
605   https://doi.org/10.1016/j.atmosenv.2020.117712, 2019.

606   Li, Y. C., Liu, J., Han, H., Zhao, T. L., Zhang, X., Zhuang, B. L., Wang, T. J., Chen, H. M., Wu, Y.,
607   and Li, M. M.: Collective impacts of biomass burning and synoptic weather on surface $PM_{2.5}$
608   and CO in Northeast China, *Atmos. Environ.*, 213, 64–80,
609   https://doi.org/10.1016/j.atmosenv.2019.05.062, 2019.

610   Li, Y. R., Tan, Z. Q., Ye, C. X., Wang, J. X., Wang, Y. W., Zhu, Y., Liang, P. F., Chen, X., Fang, Y.
611   H., Han, Y. Q., Wang, Q., He, D., Wang, Y., and Zhu, T.: Using wavelet transform to analyse
612   on-road mobile measurements of air pollutants: a case study to evaluate vehicle emission
613   control policies during the 2014 APEC summit, *Atmos. Chem. Phys.*, 19, 13841–13857,
614   https://doi.org/10.5194/acp-19-13841-2019, 2019.

615   Lian, X. B., Huang, J. P., Huang, R. J., Liu, C. W., Wang, L. N., and Zhang, T. H.: Impact of city
616   lockdown on the air quality of COVID-19-hit of Wuhan city, *Sci. Total Environ.*, 742, 140556,
617   https://doi.org/10.1016/j.scitotenv.2020.140556, 2020.

618   Lin, P., Aiona, P. K., Li, Y., Shiraiwa, M., Laskin, J., Nizkorodov, S. A., and Laskin, A.: Molecular
619   characterization of brown carbon in biomass burning aerosol particles, *Environ. Sci. Technol.*,
620   50, 11815–11824, https://doi.org/10.1021/acs.est.6b03024, 2016.

621   Lin, P., Bluvshtein, N., Rudich, Y., Nizkorodov, S. A., Laskin, J., and Laskin, A.: Molecular
622   chemistry of atmospheric brown carbon inferred from a nationwide biomass burning event,
623   *Environ. Sci. Technol.*, 51, 11561–11570, https://doi.org/10.1021/acs.est.7b02276, 2017.

624   Lin, P., Fleming, L. T., Nizkorodov, S. A., Laskin, J., and Laskin, A.: Comprehensive molecular
625   characterization of atmospheric brown carbon by high resolution mass spectrometry with
626   electrospray and atmospheric pressure photoionization, *Anal. Chem.*, 90, 12493–12502,
627   https://doi.org/10.1021/acs.analchem.8b02177, 2018.

628   Lin, P., Laskin, J., Nizkorodov, S. A., and Laskin, A.: Revealing brown carbon chromophores
629   produced in reactions of methylglyoxal with ammonium sulfate, *Environ. Sci. Technol.*, 49,
630   14257–14266, https://doi.org/10.1021/acs.est.5b03608, 2015.

631   Liu, T. Y., Chan, A. W. H., and Abbatt, J. P. D.: Multiphase oxidation of sulfur dioxide in aerosol
632   particles: implications for sulfate formation in polluted environments, *Environ. Sci. Technol.*,

8, 4227–4242, https://doi.org/10.1021/acs.est.0c06496, 2021.

Liu, X. X., Zhang, Y., Huey, L. G., Yokelson, R. J., Wang, Y., Jimenez, J. L., Campuzano-Jost, P., Beyersdorf, A. J., Blake, D. R., Choi, Y., St Clair, J. M., Crounse, J. D., Day, D. A., Diskin, G. S., Fried, A., Hall, S. R., Hanisco, T. F., King, L. E., Meinardi, S., Mikoviny, T., Palm, B. B., Peischl, J., Perring, A. E., Pollack, I. B., Ryerson, T. B., Sachse, G., Schwarz, J. P., Simpson, I. J., Tanner, D. J., Thornhill, K. L., Ullmann, K., Weber, R. J., Wennberg, P. O., Wisthaler, A., Wolfe, G. M., and Ziemba, L. D.: Agricultural fires in the southeastern U.S. during SEAC⁴RS: emissions of trace gases and particles and evolution of ozone, reactive nitrogen, and organic aerosol, *J. Geophys. Res. Atmos.*, 121, 7383–7414, https://doi.org/10.1002/2016JD025040, 2016.

McClure, C. D., Lim, C. Y., Hagan, D. H., Kroll, J. H., and Cappa, C. D.: Biomass-burning-derived particles from a wide variety of fuels – Part 1: properties of primary particles, *Atmos. Chem. Phys.*, 20, 1531–1547, https://doi.org/10.5194/acp-20-1531-2020, 2020.

McMeeking, G. R., Kreidenweis, S. M., Baker, S., Carrico, C. M., Chow, J. C., Collett Jr., J. L., Hao, W. M., Holden, A. S., Kirchstetter, T. W., Malm, W. C., Moosmüller, H., Sullivan, A. P., and Wold, C. E.: Emissions of trace gases and aerosols during the open combustion of biomass in the laboratory, *J. Geophys. Res.*, 114, D19210, https://doi.org/10.1029/2009JD011836, 2009.

Mohr, C., Lopez-Hilfiker, F. D., Zotter, P., Prévôt, A. S. H., Xu, L., Ng, N. L., Herndon, S. C., Williams, L. R., Franklin, J. P., Zahniser, M. S., Worsnop, D. R., Knighton, W. B., Aiken, A. C., Gorkowski, K. J., Dubey, M. K., Allan, J. D., and Thornton, J. A.: Contribution of nitrated phenols to wood burning brown carbon light absorption in Detling, United Kingdom during winter time, *Environ. Sci. Technol.*, 47, 6316–6324, https://doi.org/10.1021/es400683v, 2013.

Ni, H. Y., Huang, R. J., Pieber, S. M., Corbin, J. C., Stefenelli, G., Pospisilova, V., Klein, F., Gysel-Beer, M., Yang, L., Baltensperger, U., El Haddad, I., Slowik, J. G., Cao, J. J., Prévôt, A. S. H., and Dusek, U.: Brown carbon in primary and aged coal combustion emission, *Environ. Sci. Technol.,* 55, 5701–5710, https://doi.org/10.1021/acs.est.0c08084, 2021.

Pokhrel, R. P., Wagner, N. L., Langridge, J. M., Lack, D. A., Jayarathne, T., Stone, E. A., Stockwell, C. E., Yokelson, R. J., and Murphy, S. M.: Parameterization of single-scattering albedo (SSA) and absorption Ångström exponent (AAE) with EC/OC for aerosol emissions from biomass burning, *Atmos. Chem. Phys.*, 16, 9549–9561, https://doi.org/10.5194/acp-16-9549-2016, 2016.

Saleh, R.: From measurements to models: toward accurate representation of brown carbon in climate calculations, *Curr. Pollut. Rep.*, 6, 90–104, https://doi.org/10.1007/s40726-020-00139-3, 2020.

Salvador, C. M. G., Tang, R. Z., Priestley, M., Li, L. J., Tsiligiannis, E., Le Breton, M., Zhu, W. F.,

667   Zeng, L. M., Wang, H., Yu, Y., Hu, M., Guo, S., and Hallquist, M.: Ambient nitro-aromatic
668   compounds – biomass burning versus secondary formation in rural China, *Atmos. Chem. Phys.*,
669   21, 1389–1406, https://doi.org/10.5194/acp-21-1389-2021, 2021.

670   Sand, M., Samset, B. H., Myhre, G., Gliβ, J., Bauer, S. E., Bian, H. S., Chin, M., Checa-Garcia, R.,
671   Ginoux, P., Kipling, Z., Kirkevåg, A., Kokkola, H., Le Sager, P., Lund, M. T., Matsui, H., van
672   Noije, T., Olivié, D. J. L., Remy, S., Schulz, M., Stier, P., Stjern, C. W., Takemura, T., Tsigaridis,
673   K., Tsyro, S. G., and Watson-Parris, D.: Aerosol absorption in global models from AeroCom
674   phase III, *Atmos. Chem. Phys.*, 21, 15929–15947, https://doi.org/10.5194/acp-21-15929-2021,
675   2021.

676   Shen, X. B., Hao, J. T., Kong, L., Shi, Y., Cao, X. Y., Shi, J. C., Yao, Z. L., Li, X., Wu, B. B., Xu, Y.
677   M., and He, K. B.: Variation characteristics of fine particulate matter and its components in
678   diesel vehicle emission plumes, *J. Environ. Sci.*, 107, 138–149,
679   https://doi.org/10.1016/j.jes.2021.01.034, 2021.

680   Su, H., Cheng, Y. F., and Pöschl, U.: New multiphase chemical processes influencing atmospheric
681   aerosols, air quality, and climate in the Anthropocene, *Acc. Chem. Res.*, 53, 2034–2043,
682   https://doi.org/10.1021/acs.accounts.0c00246, 2020.

683   Tabazadeh, A., Djikaev, Y. S., and Reiss, H.: Surface crystallization of supercooled water in clouds,
684   *Proc. Natl. Acad. Sci. USA*, 99, 15873–15878, https://doi.org/10.1073/pnas.252640699, 2002.

685   Wang, Q. Q., Zhou, Y. Y., Ma, N., Zhu, Y., Zhao, X. C., Zhu, S. W., Tao, J. C., Hong, J., Wu, W. J.,
686   Cheng, Y. F., and Su, H.: Review of brown carbon aerosols in China: pollution level, optical
687   properties, and emissions, *J. Geophys. Res. Atmos.*, 127, e2021JD035473,
688   https://doi.org/10.1029/2021JD035473, 2022.

689   Wang, Y. S., Li, W. J., Gao, W. K., Liu, Z. R., Tian, S. L., Shen, R. R., Ji, D. S., Wang, S., Wang, L.
690   L., Tang, G. Q., Song, T., Cheng, M. T., Wang, G. H., Gong, Z. Y., Hao, J. M., and Zhang, Y.
691   H.: Trends in particulate matter and its chemical compositions in China from 2013-2017, *Sci.*
692   *China Earth Sci.*, 62, 1857–1871, https://doi.org/10.1007/s11430-018-9373-1, 2019.

693   Washenfelder, R. A., Azzarello, L., Ball, K., Brown, S. S., Decker, Z. C. J., Franchin, A.,
694   Fredrickson, C. D., Hayden, K., Holmes, C. D., Middlebrook, A. M., Palm, B. B., Pierce, R.
695   B., Price, D. J., Roberts, J. M., Robinson, M. A., Thornton, J. A., Womack, C. C., and Young,
696   C. J.: Complexity in the evolution, composition, and spectroscopy of brown carbon in aircraft
697   measurements of wildfire plumes, *Geophys. Res. Lett.*, 49, e2022GL098951,
698   https://doi.org/10.1029/2022GL098951, 2022.

699   Wozniak, A. S., Bauer, J. E., Sleighter, R. L., Dickhut, R. M., and Hatcher, P. G.: Technical Note:
700   Molecular characterization of aerosol-derived water soluble organic carbon using ultrahigh

resolution electrospray ionization Fourier transform ion cyclotron resonance mass spectrometry, *Atmos. Chem. Phys.*, 8, 5099–5111, https://doi.org/10.5194/acp-8-5099-2008, 2008.

Wu, J., Kong, S. F., Yan, Y. Y., Yao, L. Q., Yan, Q., Liu, D. T., Shen, G. F., Zhang, X. Y., and Qi, S. H.: Neglected biomass burning emissions of air pollutants in China-views from the corncob burning test, emission estimation, and simulations, *Atmos. Environ.*, 278, 119082, https://doi.org/10.1016/j.atmosenv.2022.119082, 2022.

Xie, M. J., Chen, X., Hays, M. D., and Holder, A. L.: Composition and light absorption of N-containing aromatic compounds in organic aerosols from laboratory biomass burning, *Atmos. Chem. Phys.*, 19, 2899–2915, https://doi.org/10.5194/acp-19-2899-2019, 2019.

Xie, M. J., Zhao, Z. Z., Holder, A. L., Hays, M. D., Chen, X., Shen, G. F., Jetter, J. J., Champion, W. M., and Wang, Q. G.: Chemical composition, structures, and light absorption of N-containing aromatic compounds emitted from burning wood and charcoal in household cookstoves, *Atmos. Chem. Phys.*, 20, 14077–14090, https://doi.org/10.5194/acp-20-14077-2020, 2020.

Xu, J. Z., Hettiyadura, A. P. S., Liu, Y. M., Zhang, X. H., Kang, S. C., and Laskin, A.: Atmospheric brown carbon on the Tibetan Plateau: regional differences in chemical composition and light absorption properties, *Environ. Sci. Technol. Lett.*, 9, 219−225, https://doi.org/10.1021/acs.estlett.2c00016, 2022.

Yang, M., Howell, S. G., Zhuang, J., and Huebert, B. J.: Attribution of aerosol light absorption to black carbon, brown carbon, and dust in China - Interpretations of atmospheric measurements during EAST-AIRE, *Atmos. Chem. Phys.*, 9, 2035–2050, https://doi.org/10.5194/acp-9-2035-2009, 2009.

Yttri, K. E., Schnelle-Kreis, J., Maenhaut, W., Abbaszade, G., Alves, C., Bjerke, A., Bonnier, N., Bossi, R., Claeys, M., Dye, C., Evtyugina, M., Garcá-Gacio, D., Hillamo, R., Hoffer, A., Hyder, M., Iinuma, Y., Jaffrezo, J. L., Kasper-Giebl, A., Kiss, G., Lopez-Mahia, P. L., Pio, C., Piot, C., Ramirez-Santa-Cruz, C., Sciare, J., Teinilä, K., Vermeylen, R., Vicente, A., and Zimmermann, R.: An intercomparison study of analytical methods used for quantification of levoglucosan in ambient aerosol filter samples, *Atmos. Meas. Tech.*, 8, 125–147, https://doi.org/10.5194/amt-8-125-2015, 2015.

Yuan, Q., Qi, B., Hu, D. Y., Wang, J. J., Zhang, J., Yang, H. Q., Zhang, S. S., Liu, L., Xu, L., and Li, W. J.: Spatiotemporal variations and reduction of air pollutants during the COVID-19 pandemic in a megacity of Yangtze River Delta in China, *Sci. Total Environ.*, 751, 141820, https://doi.org/10.1016/j.scitotenv.2020.141820, 2021.

735 Zeng, L. H., Dibb, J., Scheuer, E., Katich, J. M., Schwarz, J. P., Bourgeois, I., Peischl, J., Ryerson,
736   T., Warneke, C., Perring, A. E., Diskin, G. S., DiGangi, J. P., Nowak, J. B., Moore, R. H.,
737   Wiggins, E. B., Pagonis, D., Guo, H. Y., Campuzano-Jost, P., Jimenez, J. L., Xu, L., and Weber,
738   R. J.: Characteristics and evolution of brown carbon in western United States wildfires, *Atmos.*
739   *Chem. Phys.*, 22, 8009–8036, https://doi.org/10.5194/acp-22-8009-2022, 2022.

740 Zeng, L. H., Zhang, A. X., Wang, Y. H., Wagner, N. L., Katich, J. M., Schwarz, J. P., Schill, G. P.,
741   Brock, C., Froyd, K. D., Murphy, D. M., Williamson, C. J., Kupc, A., Scheuer, E., Dibb, J., and
742   Weber, R. J.: Global measurements of brown carbon and estimated direct radiative effects,
743   *Geophys. Res. Lett.*, 47, e2020GL088747, https://doi.org/10.1029/2020GL088747, 2020.

744 Zeng, Y. L., Ning, Y. L., Shen, Z. X., Zhang, L. M., Zhang, T., Lei, Y. L., Zhang, Q., Li, G. H., Xu,
745   H. M., Ho, S. S. H., and Cao, J. J.: The roles of N, S, and O in molecular absorption features
746   of brown carbon in $PM_{2.5}$ in a typical semi-arid megacity in Northwestern China, *J. Geophys.*
747   *Res. Atmos.*, 126, e2021JD034791, https://doi.org/10.1029/2021JD034791, 2021.

748 Zhang, J., Smith, K. R., Ma, Y., Ye, S., Jiang, F., Qi, W., Liu, P., Khalil, M. A. K., Rasmussen, R.
749   A., and Thorneloe, S. A.: Greenhouse gases and other airborne pollutants from household
750   stoves in China: a database for emission factors, *Atmos. Environ.*, 34, 4537–4549,
751   https://doi.org/10.1016/S1352-2310(99)00450-1, 2000.

752 Zhang, Y. L., Wang, X. M., Li, G. H., Yang, W. Q., Huang, Z. H., Zhang, Z., Huang, X. Y., Deng,
753   W., Liu, T. Y., Huang, Z. Z., and Zhang, Z. Y.: Emission factors of fine particles, carbonaceous
754   aerosols and traces gases from road vehicles: recent tests in an urban tunnel in the Pearl River
755   Delta, China, *Atmos. Environ.*, 122, 876–884, https://doi.org/10.1016/j.atmosenv.2015.08.024,
756   2015.
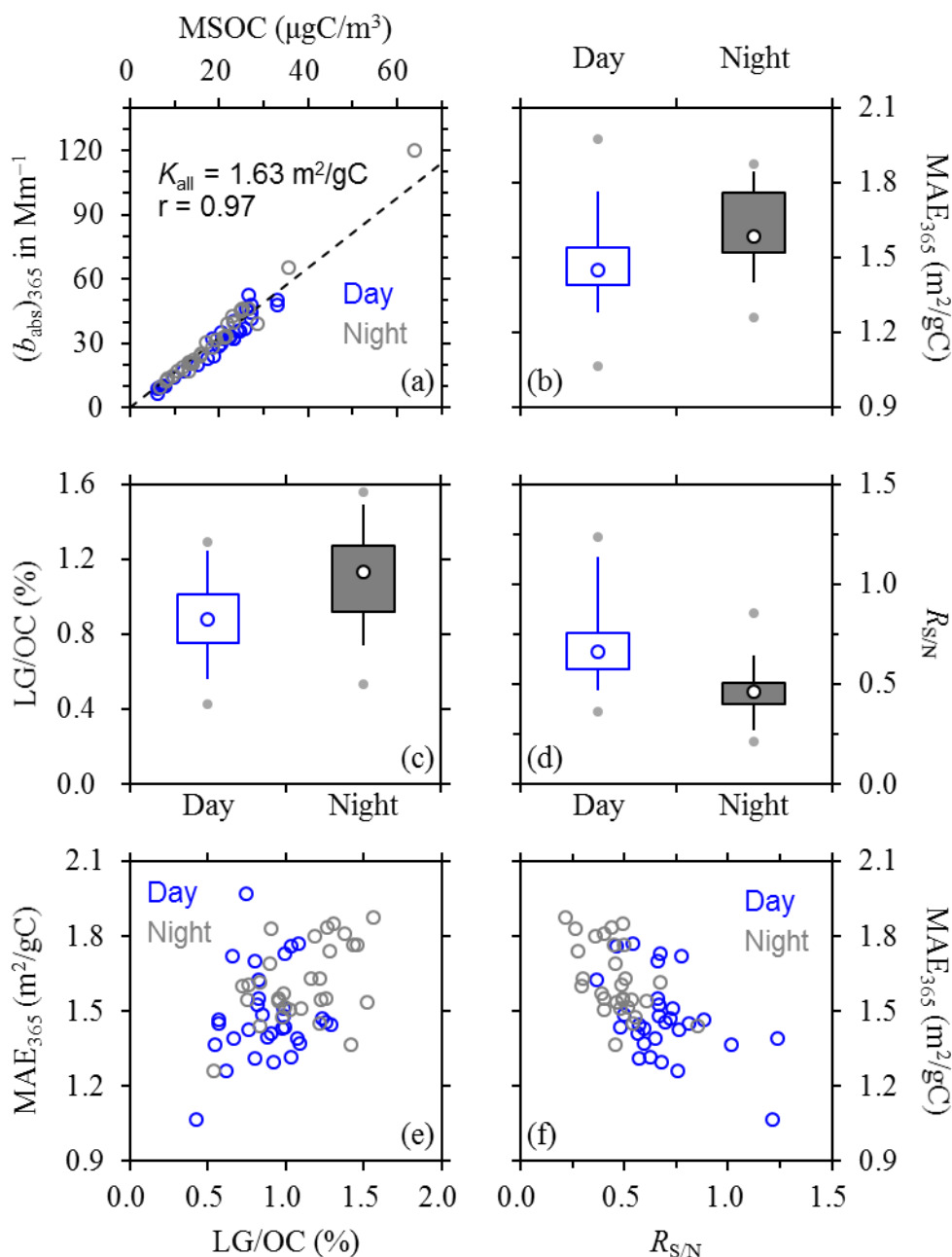
Figure 1. (a) Dependence of $(b_{abs})_{365}$ on MSOC, **(b–d)** diurnal variations of MAE$_{365}$, LG/OC (on a basis of carbon mass) and $R_{S/N}$, and **(e–f)** dependences of MAE$_{365}$ on LG/OC or $R_{S/N}$ during winter. In (a), the dashed line indicates linear regression result based on all the winter samples, with K_{all} as slope (intercept was set as zero). In (b-d), lower and upper box bounds indicate the 25th and 75th percentiles, the whiskers below and above the box indicate the 5th and 95th percentiles, the solid circles below and above the box indicate the minimum and maximum, and the open circle within the box marks the median (the same hereinafter). Comparison of (e) and (f) suggests that the wintertime MAE$_{365}$ was more strongly influenced by $R_{S/N}$ compared to LG/OC. The dependence shown in (f) could be approximated by the following function for all the winter samples ($r = 0.61$):

MAE$_{365}$ = $(-0.51 \pm 0.09) \times R_{S/N} + (1.84 \pm 0.05)$.

768
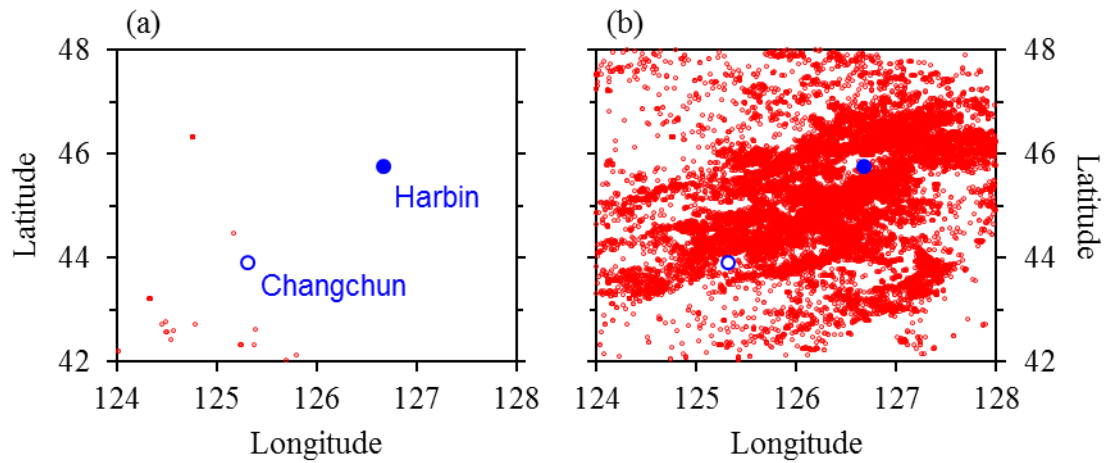
Figure 2. Cumulative fire hotspots ~~Active fires (red circles)~~ detected ~~during~~ throughout the **(a)** winter and **(b)** spring measurement periods around Harbin, with their locations shown by the red circles. ~~The location of another central city of the HC metropolitan area, Changchun, is also shown.~~ The HC metropolitan area has two central cities as marked by the blue circles. The fire data were based on the joint NASA/NOAA Suomi National Polar-orbiting Partnership (S-NPP) satellite, and were downloaded from the Fire Information for Resource Management System (FIRMS; https://firms.modaps.eosdis.nasa.gov/, last access: 1 January, 2023).
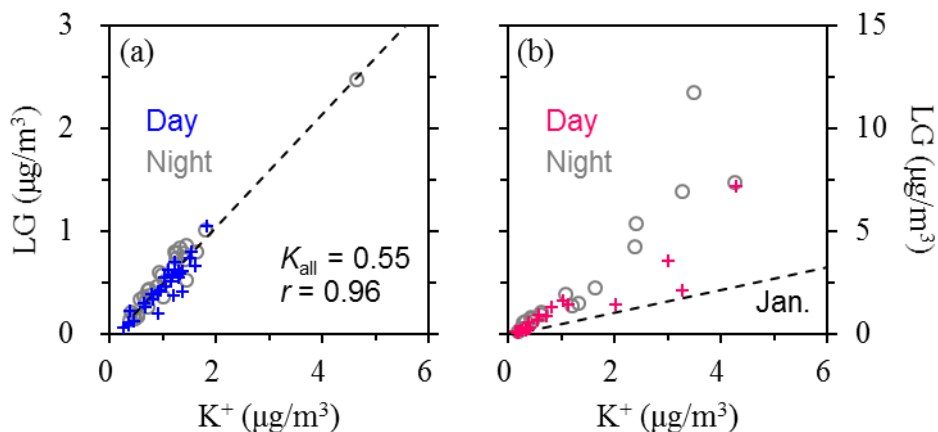
Figure 3. Dependences of levoglucosan on K^+ during **(a)** winter and **(b)** spring. In (a), the dashed line indicates linear regression result based on all the winter samples, with K_{all} as slope. The regression line of winter campaign is also shown in (b) for comparison to highlight the increased and variable LG/K^+ ratios in spring. The relatively low and constant LG/K^+ in winter were attributed to residential burning of crop residues, a routine activity occurring every day in rural areas for cooking and heating. The higher LG/K^+ in spring were associated with agricultural fires, as supported by the intensive fire hotspots detected.
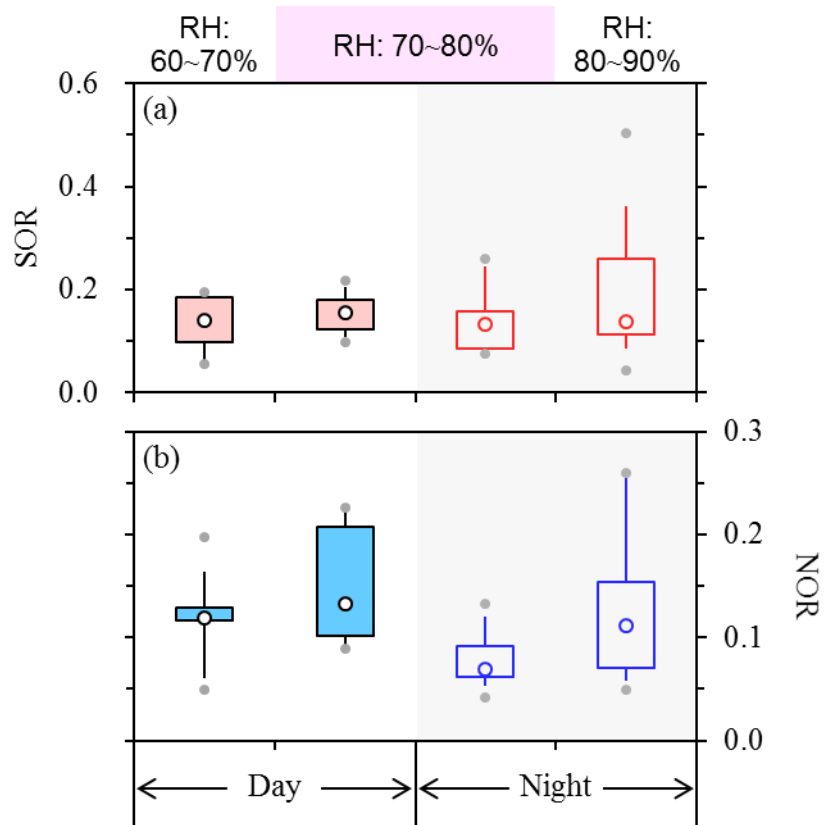
784

785 **Figure 4.** Diurnal variations of **(a)** SOR and **(b)** NOR in winter, with results from different RH
786 ranges shown separately. Daytime and nighttime samples had ~~the same~~ a common RH range of 70–
787 80%, whereas low RH levels of 60–70% and high RH levels of 80–90% occurred only during the
788 day and at night, respectively.

789
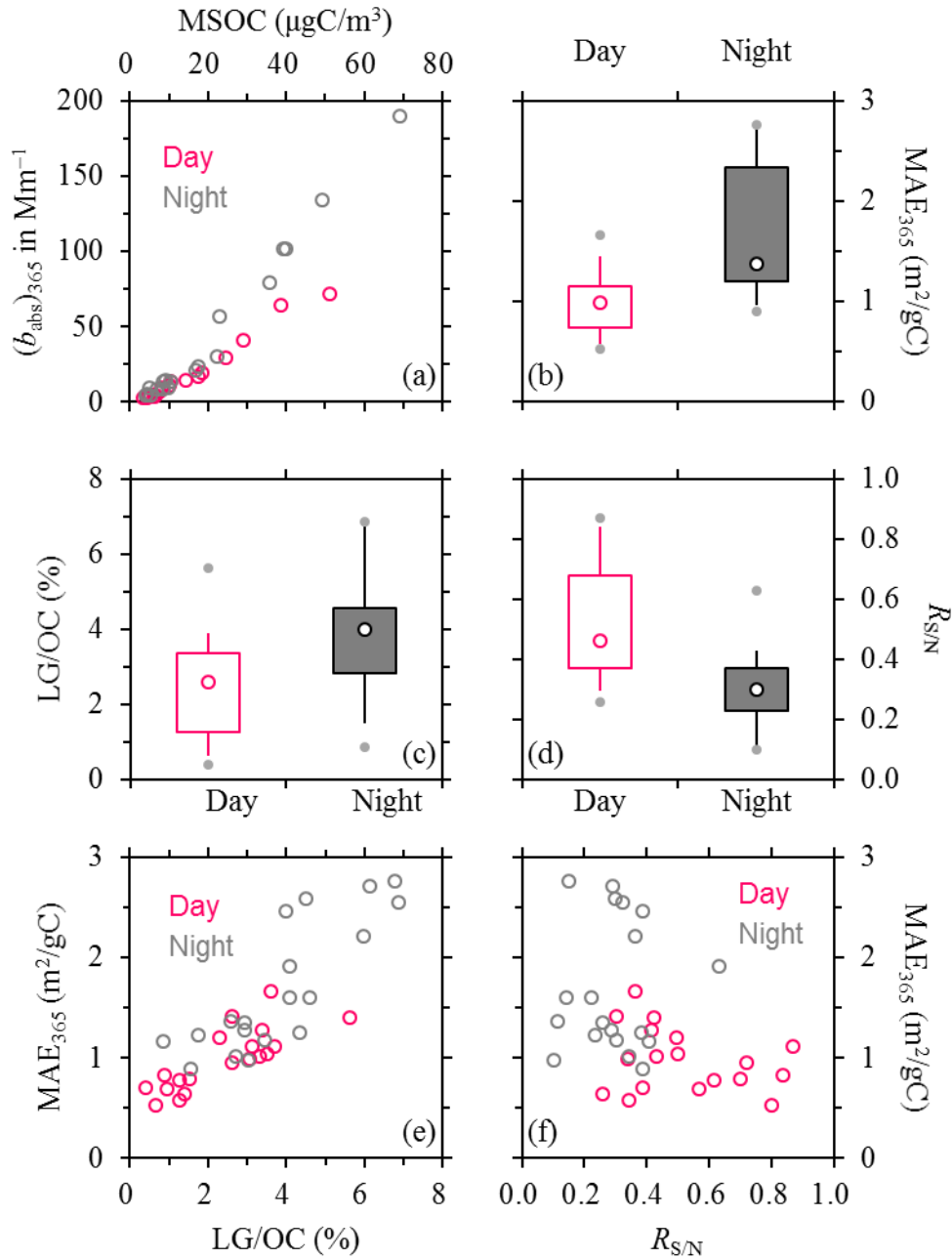
Figure 5. The same as Figure 1 but for spring. MAE_{365} showed more pronounced diurnal variations in spring than winter, although the daytime vs. nighttime discrepancies in $R_{S/N}$ were comparable between the two seasons. Comparison of (e) and (f) suggests that unlike winter, the springtime MAE_{365} was more strongly influenced by LG/OC than by $R_{S/N}$. The dependence shown in (e) could be approximated by the following function for all the spring samples ($r = 0.84$): $MAE_{365} = (30.48 \pm 3.28) \times LG/OC + (0.39 \pm 0.12)$, where LG/OC is on a basis of carbon mass and in %.
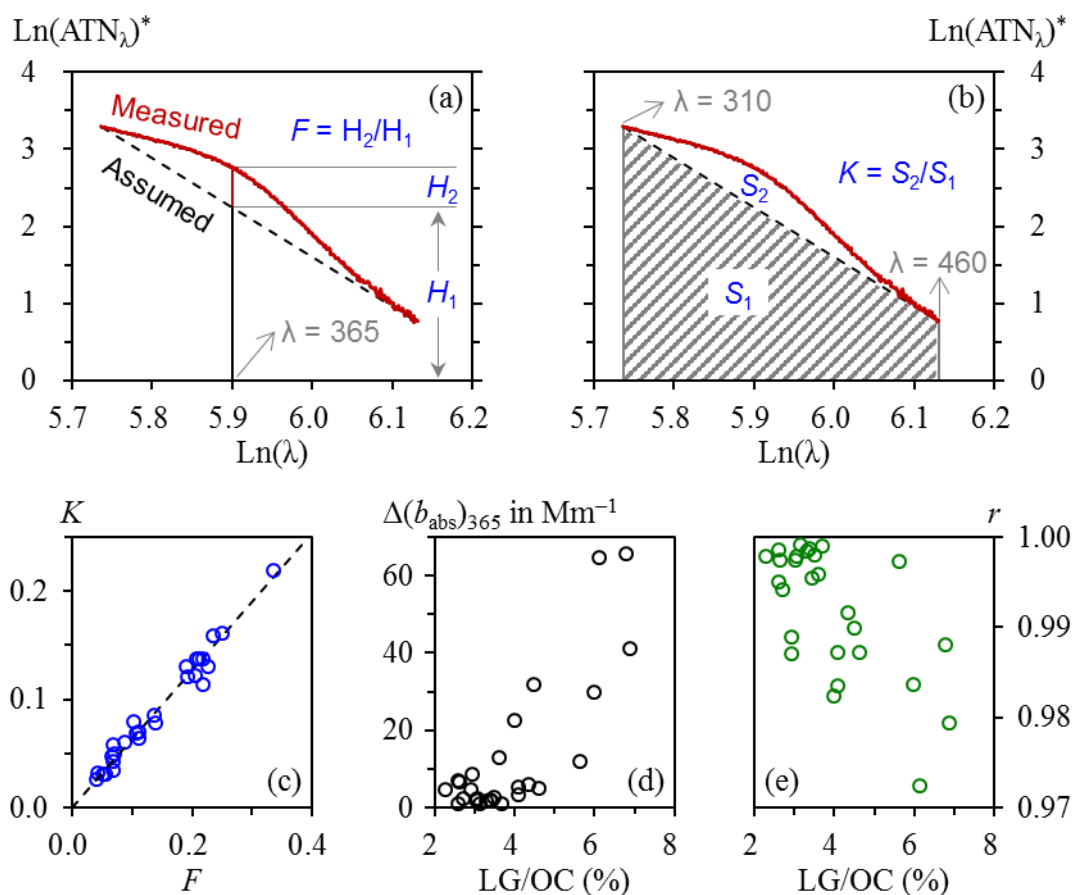
Figure 6. Nonlinearity of $\ln(ATN_\lambda)^*$ on $\ln(\lambda)$ during agricultural fire episodes in spring: **(a–b)** illustrations of the determination of F and K, **(c)** comparison of K and F, and **(d–e)** dependences of $\Delta(b_{abs})_{365}$ and r on LG/OC. In (a) and (b), the measured spectrum correspond to the nighttime sample collected on April 21, 2021, which had an LG/OC of 6.87%; the assumed spectrum was generated by drawing a line between the two points with x values of $\ln(310)$ and $\ln(460)$; H_1 indicates $\ln(ATN_{365})^*$ of the assumed spectrum, while H_2 indicates the difference in $\ln(ATN_{365})^*$ between the two spectra; S_1 indicates the area enclosed by the assumed spectrum and the x-axis, while S_2 indicates the area enclosed between the two spectra. In (c), the dashed line indicates linear regression result (intercept was set as zero) and the corresponding r value was 0.99. In (e), r was derived from linear regression of $\ln(ATN_\lambda)^*$ on $\ln(\lambda)$. Although the r values seemed reasonable, the AAE results should be interpreted with caution given the apparent absorption peak at ~365 nm.
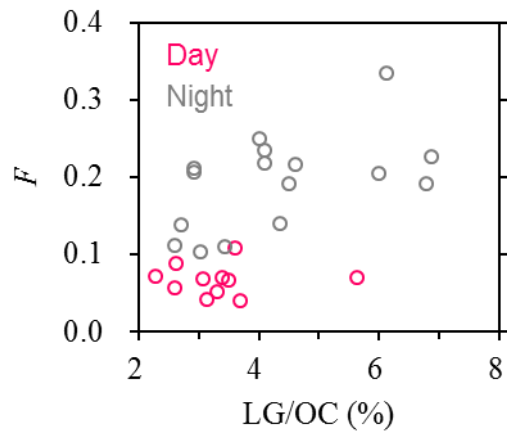
808

809 **Figure 7.** Dependence of F, a measure of the significance of the ~365 nm absorption peak, on
810 LG/OC during agricultural fire episodes in spring. For a given LG/OC range, F decreased
811 substantially during the day, likely due to photo-bleaching of chromophores associated with the
812 ~365 nm peak. The same conclusion could be reached based on K, another indicator for the
813 significance of the ~365 nm peak.